Bead–Spring Model Calculations of the Viscoelastic and Oscillatory Flow Birefringence Properties of Block Copolymer Solutions

Victor F. Man† and John L. Schrag*

Department of Chemistry and Rheology Research Center, University of Wisconsin, Madison, Wisconsin 53706

Timothy P. Lodge

Department of Chemistry, University of Minnesota, Minneapolis, Minnesota 55455

Received August 8, 1990; Revised Manuscript Received December 29, 1990

ABSTRACT: Bead–spring model (BSM) calculations of the polymer contributions to viscoelastic (VE) and oscillatory flow birefringence (OFB) properties of very dilute block copolymer solutions are reported. The original BSM of Rouse and Zimm has been extended to the case of diblock and triblock copolymers, following the model of Wang. The VE properties have been determined via exact calculations of the eigenvalues of the modified $\tilde{H}\cdot\tilde{A}$ matrix, and the OFB properties from the exact eigenvalues and eigenvectors of this matrix; the eigenvectors are required in order to calculate optical weighting factors for each of the normal modes, which depend strongly on the relative values of the optical constants for the various blocks. Different optical constants for different blocks lead to a different effective stress-optic coefficient for each normal mode. Illustrative calculations for four different situations are presented. In all cases, the VE properties are not substantially altered from the homopolymer case. The OFB properties, however, can vary strikingly with modest changes in model parameters due to the mode-dependent optical weighting factors. For chains in which the optical factors for the blocks differ in sign, the OFB properties have frequency dependences that are much more featured than for their homopolymer equivalents, which offers the possibility that OFB measurements of block copolymer solutions may provide extremely powerful and unique characterization information including block lengths and locations. Both mechanically uniform and nonuniform block copolymers have been considered; it is found that small variations between subchain friction coefficients can lead to substantially more striking frequency dependences for OFB properties than are predicted for mechanically uniform chains.

I. Introduction

Block copolymers constitute a class of macromolecules that exhibits a rich variety of structural and dynamic behavior. In the bulk state, attention has been focused on the several morphologies that result from phase separation on the microscopic scale, and more recently on the dynamics of the separation process itself.[1] In solution, the effect of interblock repulsion on the chain conformation and hydrodynamics has been extensively examined.[2] Nevertheless, a detailed understanding of many block copolymer phenomena has not been achieved. One class of experiments that has not yet been exploited fully in this context is that which senses conformational dynamics over a wide frequency range, in particular the linear viscoelastic (VE) and oscillatory flow birefringence (OFB) techniques.

The conformational dynamics of linear and branched homopolymers in dilute solutions have been examined extensively over the past 20 years, via both VE and OFB approaches.[3,4] By extrapolation to infinite dilution, it has been possible to interpret the results in terms of bead–spring models (BSM);[5,6] in general, such models are able to describe the data extremely well, at least at low and moderate frequencies and for small numbers of branches. At the same time, efficient algorithms have been developed to compute exactly the predicted relaxation time spectra and thus the VE and OFB properties.[7-11] These algorithms are able to accommodate a wide variety of chain topologies, values of N (the number of bead–spring units in the model chain) exceeding 10^3, arbitrary values of h^* (the hydrodynamic interaction parameter), and excluded volume in various approximate forms. If extended to block copolymer systems, this approach offers the potential of investigating in detail (i) the effect of interblock interactions on chain dynamics, (ii) the possibility of extracting unique characterization information with regard to block length and location, and (iii) the contribution of different portions of the chain to the total chain relaxation response.

In an earlier study, Soli[12] examined the OFB properties of polystyrene (PS)–polyisoprene (PI) and PS–polybutadiene (PB) block copolymers in Aroclor 1248, a viscous solvent employed extensively in similar measurements. The results appeared to be highly unusual and were completely unlike any homopolymer system examined. In particular, it was clear that the relaxation spectrum alone did not control the solution response. Concurrently, Wang presented a model for the VE and OFB properties of a general A–B–C triblock copolymer in solution.[13,14] This model was a direct extension of that originally developed by Rouse[5] and Zimm;[6] the parameters N, b (the root-mean-square spring length), and ρ (the bead friction coefficient) would adopt different values for each block. Using an extension of the exact eigenvalue algorithm developed by Lodge and Wu,[7,8] Wang computed the VE properties for a variety of chain compositions.[13,14] In general, however, the results were not strikingly different from those for a homopolymer of similar total length. The calculation of the OFB properties required specification of the optical parameter q for each block, where q is directly

† Present address: Ecolab Inc., Research Center, Mendota Heights, MN 55118.

0024-9297/91/2224-3666$02.50/0

proportional to a stress-optic coefficient, and also required determination of the eigenvectors (i.e., the normal modes) for the model chain. The contribution of each normal mode to the total polymer OFB incorporates a mode-dependent weighting factor, in contrast to VE properties for which all modes are weighted equally. The normal modes were only calculated for mechanically uniform chains in the free-draining limit ($h^* = 0$), and OFB properties were only computed over a limited frequency range. Nevertheless, these results suggested that some of the features apparent in Soli's data were the result of the difference in sign between q for PS and for the polydienes. However, it was not possible to bring theory and experiment into reasonable agreement, even by arbitrary adjustments to parameter values.

More recently, Man and Schrag examined the VE properties of the same solutions employed by Soli.[15] These measurements confirmed that the integrity of the solutions was not an issue; however, it was equally clear that the contribution of the solvent to the measured solution properties was not being assessed correctly, and that this was a major source of difficulty in interpreting both VE and OFB results. Subsequently, this interesting issue has been examined in much more detail,[15,18] but it is not particularly relevant to the remainder of this paper. With this solvent contribution established, however, it became possible to bring the block copolymer BSM predictions into much more reasonable agreement with experiment, as shown by Man.[15,18] This necessitated the exact computation of the OFB properties and, therefore, of the normal modes and the mode-dependent weighting factors.

In this paper, we describe detailed calculations of the VE and OFB properties of diblock and triblock chains at infinite dilution, following the model of Wang. In the next section, the block copolymer BSM is reviewed, and the computational scheme outlined. Results are then presented for selected interesting situations, emphasizing the OFB results, which, as noted by Wang, can be strikingly different from the corresponding VE properties. Two cases are of particular interest. In one, only a single chain segment has a nonzero q and thus contributes to the OFB properties. This makes it possible to establish the relative contributions of different portions of the chain to the total chain response at any given frequency, by varying the location of the "visible" segment. In the other, two-component copolymers (e.g., diblocks and symmetric triblocks) for which the two q values differ in sign exhibit highly featured frequency dependences, especially when the two components also have different frictional properties. The results are also compared to previous calculations of the VE properties of free-draining block copolymer chains. In a subsequent paper, experimental OFB and VE results for PS–PI and PS–PB block copolymers will be compared with model calculations.[18]

II. Theory

A. Basic BSM Formulation for a Linear Homopolymer. The bead–spring model of a flexible homopolymer assumes that a chain may be considered in terms of a number of Gaussian submolecules, each represented by a bead-and-spring element, so that a linear homopolymer molecule is modeled as a freely jointed chain of $(N + 1)$ identical beads joined by N identical "entropic" Hookean springs (force constant $3k_BT/b^2$, where k_B is the Boltzmann constant, T the absolute temperature, and b^2 the mean-square spring length). The beads (bead friction coefficient ρ) experience a Stokes-like hydrodynamic drag as they move through the solvent, which is modeled as a Newtonian continuum with viscosity η_e; in general, η_e is different from η_s, the viscosity of the pure solvent.[16,17]

Following the original formulation of Rouse[5] and Zimm,[6] and incorporating hydrodynamic interaction via the approximate form of Kirkwood and Riseman,[19] the equation for the x component of the chain motion can be written as

$$d\tilde{x}/dt = \tilde{v}_x + (1/\rho)\tilde{\tilde{H}}\cdot\tilde{F}_x = \tilde{v}_x - (k_BT/\rho)\tilde{\tilde{H}}\cdot(\partial/\partial\tilde{x}) \ln \psi - (3k_BT/(b^2\rho))\tilde{\tilde{H}}\cdot\tilde{\tilde{A}}\cdot\tilde{x} \quad (1)$$

with

$$d\tilde{x}/dt = (dx_0/dt, dx_1/dt, ..., dx_N/dt)^T \quad (2)$$

$$\tilde{v}_x = (v_{x0}, v_{x1}, ..., v_{xN})^T \quad (3)$$

$$\tilde{F}_x = (F_{x0}, F_{x1}, ..., F_{xN})^T \quad (4)$$

$$\tilde{x} = (x_0, x_1, ..., x_N)^T \quad (5)$$

where dx_j/dt is the x component of the velocity of the jth bead, v_{xj} is the x component of the velocity that the fluid would have at the position of j if the bead were absent, F_{xj} is the x component of the force acting on the jth bead, x_j is the x component of the location of the jth bead, and $\psi(x_0, y_0, ..., z_N)$ is the distribution function, which is the probability of finding each bead j with coordinates between x_j and $x_j + dx_j$, y_j and $y_j + dy_j$, z_j and $z_j + dz_j$.

The eigenvalues λ_k of the $\tilde{\tilde{H}}\cdot\tilde{\tilde{A}}$ matrix are related to the relaxation times τ_k of the normal modes of motion of the model chain by $\tau_k = b^2\rho/6k_BT\lambda_k$. Predictions for the chain contributions to VE and OFB properties (at low shear rates) are given by the following equations for the modified reduced intrinsic shear moduli $[G']_{PR}$ and $[G'']_{PR}$, and the intrinsic magnitude $[S_m]_P$ and phase angle $[\theta]_P$ of the modified mechano-optic coefficient S_P^*, obtained by subtracting the contribution from the chain environment ($G_e^* = i\omega\eta_e^*$ and S_e^*):

$$[G']_{PR} = \frac{M}{RT}[G']_P = \frac{M}{RT}\lim_{c\to 0}\left(\frac{G' - G'_e}{c}\right) = (\omega\tau_1)^2\sum_k(\tau_k/\tau_1)^2/[1 + (\omega\tau_1)^2(\tau_k/\tau_1)^2] \quad (6a)$$

$$[G'']_{PR} = \frac{M}{RT}[G'']_P = \frac{M}{RT}\lim_{c\to 0}\left(\frac{G'' - G''_e}{c}\right) = \frac{M}{RT}\lim_{c\to 0}\left(\frac{G'' - \omega\eta'_e}{c}\right) = (\omega\tau_1)\sum_k(\tau_k/\tau_1)/[1 + (\omega\tau_1)^2(\tau_k/\tau_1)^2] \quad (6b)$$

$$[S^*]_P = \lim_{c\to 0}\left(\frac{S^* - S_e^*}{c}\right) = \lim_{c\to 0}\left(\frac{S' - S'_e + i(S'' - S''_e)}{c}\right] = [S']_P + i[S'']_P = [S_m]_P e^{+i[\theta]_P} \quad (7a)$$

from which

$$[S_m]_P = q[(\sum_k \tau_k/(1 + \omega^2\tau_k^2))^2 + (\sum_k \omega\tau_k^2/(1 + \omega^2\tau_k^2))^2]^{1/2} \quad (7b)$$

$$[\theta]_P = \tan^{-1}([S'']_P/[S']_P) = \tan^{-1}[-[\sum_k \omega\tau_k^2/(1 + \omega^2\tau_k^2)]/[\sum_k \tau_k/(1 + \omega^2\tau_k^2)]] \quad (7c)$$

where q is an optical constant related to the index of refraction of the solvent and the intrinsic optical anisotropy of the Kuhn statistical segment.

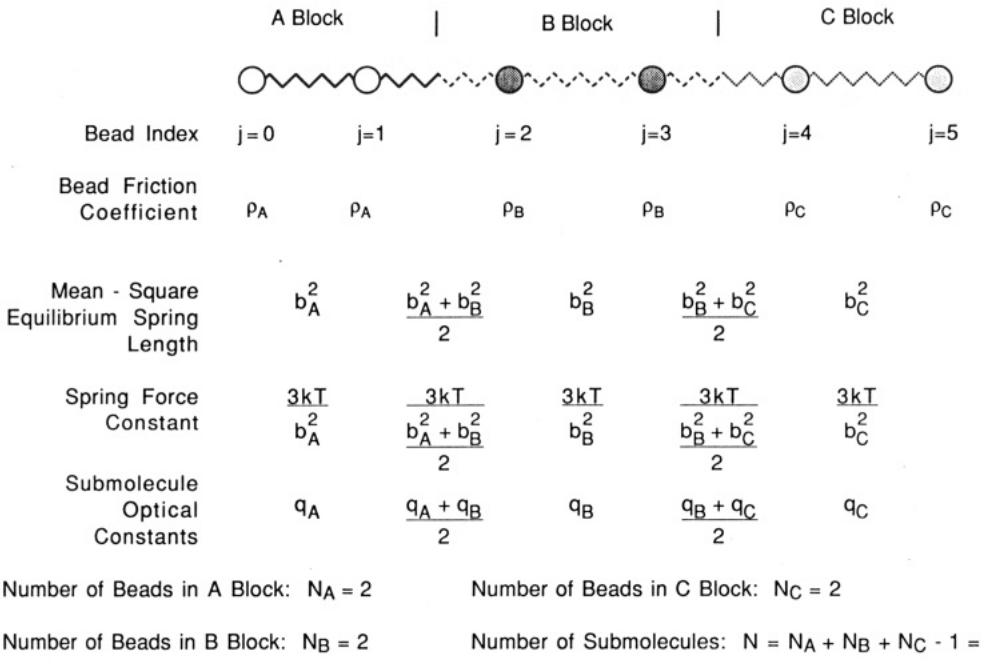

Figure 1. Illustration of a very small triblock copolymer bead–spring model chain with a listing of the various model parameters.

For homopolymers, the complex viscosity coefficient η^* and the complex mechano-optic coefficient S^* are simply related since

$$\eta^* = \frac{cRT}{M}\sum_k \frac{\tau_k}{1 + i\omega\tau_k} + \eta_e^* \tag{8}$$

and

$$S^* = \frac{cN_o qb^2}{M}\sum_k \frac{\tau_k}{1 + i\omega\tau_k} + S_e^* \tag{9}$$

where c and M are the concentration and molecular weight of the homopolymer, N_o is Avogadro's number, and η_e^* and S_e^* are the viscoelasticity and mechano-optic coefficients of the chain environment. Usually, measurement frequencies are sufficiently low such that η_e^* and S_e^* are found to be frequency-independent and real ($\eta_e^* \to \eta_e$ and $S_e^* \to S_e$). All of the above OFB relations assume that the isotropic part of the refractive index of the homopolymer matches that of the solvent to avoid form birefringence effects. The BSM thus predicts a stress-optic relation, $S^* - S_e^* = C(\eta^* - \eta_e^*)$, where C, a stress-optic coefficient, is proportional to q and is the same for the contributions from every mode.

The extent of the hydrodynamic interaction between the model beads is represented by the dimensionless hydrodynamic interaction parameter h^*, introduced by Thurston and Peterlin[20]

$$h^* = \rho/[(12\pi^3)^{1/2} b\eta_e] \tag{10}$$

which is assumed to be dependent on the polymer/solvent system but is expected to be independent of molecular weight. Although the BSM has three independent parameters, N, b^2, and ρ, the eigenvalue calculations for linear homopolymers involve only two variables, N and h^*. For finite N and nonzero h^*, the eigenvalues (λ_k) have to be calculated exactly by inverting the $\tilde{\tilde{H}}\cdot\tilde{\tilde{A}}$ matrix numerically. Exact λ_k were first computed by Thurston and Morrison[21] up to $N = 15$, and later by Lodge and Wu[7,8] up to $N = 300$. In order to compute exact λ_k for N as large as 300, Lodge and Wu introduced an $N \times N$ matrix $\tilde{\tilde{B}}$ as a more convenient alternative to Zimm's singular, nonsymmetric matrix $\tilde{\tilde{H}}\cdot\tilde{\tilde{A}}$. The basis of this is the "center of hydrodynamic resistance" transformation resulting in $\tilde{\tilde{B}}$ having only the nonzero eigenvalues of $\tilde{\tilde{H}}\cdot\tilde{\tilde{A}}$ (in other words, only the internal modes are retained). The $N \times N$ $\tilde{\tilde{B}}$ matrix, besides being nonsingular, is also symmetric, thereby reducing computer calculation time as well as increasing the upper computation limit of N (only $N(N + 1)/2$ elements of $\tilde{\tilde{B}}$ need to be stored). More recently, the accuracy of these calculations has been improved, and N has been extended to 10^4.[9-11]

B. BSM Formulation for a Linear Block Copolymer. In contrast to a homopolymer, segments of a block copolymer molecule can have different persistence lengths, different segmental friction coefficients, and different intrinsic segmental polarizability anisotropies. Any model for the prediction of block copolymer properties should address such characteristics. Furthermore, there will in general be a nonzero thermodynamic interaction (χ_{AB}) between chemically different blocks. However, just as the basic BSM is strictly applicable only to homopolymer chains in θ solvents, the possible effects of χ_{AB} on the relaxation spectrum have been ignored in this work.

Selected results of extensive BSM calculations are reported here for linear di- and triblock copolymers. The BSM formulation scheme employed is quite similar to that proposed by Wang.[13,14] For illustrative purposes, Figure 1 shows a very small model chain with a listing of the various model parameters for the different regions. Different block sizes are represented by a different number of model beads (N_A, N_B, N_C) for each block; $N + 1 = N_A + N_B + N_C$. Different block mechanical properties are represented by different equilibrium mean-square end-to-end spring lengths (b_A^2, b_B^2, b_C^2) and different bead friction coefficients (ρ_A, ρ_B, ρ_C). Assuming that random walk statistics apply throughout, the mean-square length of the spring connecting two different kinds of beads from two adjacent blocks is equal to the mean-square length of a segment formed by combining half of a submolecule from each block to form the interconnecting spring. Therefore, one has $b_{AB}^2 = (b_A^2 + b_B^2)/2$, and $b_{BC}^2 = (b_B^2 + b_C^2)/2$. The hydrodynamic interaction parameter of only the first bead type (h_A^*) needs to be specified, as those of the other types are determined by the b_i^2 and ρ_i assignments. Results for diblock copolymers can be

obtained as a special case by setting $b_B^2 = b_C^2$ and $\rho_B = \rho_C$.

(i) Equation of Motion for a Linear Block Copolymer. The calculations are based on the construction of modified matrices $\tilde{\tilde{H}}'$ and $\tilde{\tilde{A}}'$ with the above assigned parameter values to cast the equations of motion for the beads of the block copolymer model chain in matrix form:

$$d\tilde{x}/dt = \tilde{v}_x + (1/\rho_A)\tilde{\tilde{H}}'\cdot\tilde{F}_x = \tilde{v}_x - (k_BT/\rho_A)\tilde{\tilde{H}}'\cdot(\partial/\partial\tilde{x}) \times \ln\psi - (3k_BT/(b_A^2\rho_A))\tilde{\tilde{H}}'\cdot\tilde{\tilde{A}}'\cdot\tilde{x} \quad (11)$$

(ii) $\tilde{\tilde{A}}'$ Matrix for a Linear Block Copolymer. In this particular scheme, the A block is taken as the reference block; therefore ρ_A and b_A^2 are taken outside the $\tilde{\tilde{H}}'$ and $\tilde{\tilde{A}}'$ matrices in eq 11. The only nonzero elements of the symmetric tridiagonal $\tilde{\tilde{A}}'$ matrix are

$$(A'_{0,0};\ A'_{0,1}) = (1;\ -1) \quad (12a)$$

$$(A'_{j,j-1};\ A'_{jj};\ A'_{jj+1}) = (-E_j;\ E_j + E_{j+1};\ -E_{j+1}) \quad \text{for } 1 \le j \le (N-1) \quad (12b)$$

$$(A'_{N,N-1};\ A'_{N,N}) = (-E_N;\ E_N) \quad (12c)$$

where

$$E_j = 1 \quad \text{for } 1 \le j \le (N_A - 1) \quad (13a)$$

$$E_j = b_A^2/b_{AB}^2 = 2(b_A^2/b_B^2)/(1 + b_A^2/b_B^2) \quad \text{for } j = N_A \quad (13b)$$

$$E_j = b_A^2/b_B^2 \quad \text{for } (N_A + 1) \le j \le (N_A + N_B - 1) \quad (13c)$$

$$E_j = b_A^2/b_{BC}^2 = 2(b_A^2/b_B^2)(b_A^2/b_C^2)/(b_A^2/b_B^2 + b_A^2/b_C^2) \quad \text{for } j = (N_A + N_B) \quad (13d)$$

$$E_j = b_A^2/b_C^2 \quad \text{for } (N_A + N_B + 1) \le j \le N \quad (13e)$$

(iii) $\tilde{\tilde{H}}'$ Matrix for a Linear Block Copolymer. The diagonal elements of the symmetric $\tilde{\tilde{H}}'$ matrix are given by

$$H'_{jj} = 1 \quad \text{for } 0 \le j \le (N_A - 1) \quad (14a)$$

$$H'_{jj} = \rho_A/\rho_B \quad \text{for } N_A \le j \le (N_A + N_B - 1) \quad (14b)$$

$$H'_{jj} = \rho_A/\rho_C \quad \text{for } (N_A + N_B) \le j \le N \quad (14c)$$

The off-diagonal elements of the symmetric $\tilde{\tilde{H}}'$ matrix are given by

$$H'_{jk} = \rho_A T_{jk} \quad \text{for } j \ne k \quad (15)$$

where T_{jk} is the coefficient of hydrodynamic interaction between the jth and kth beads. The Kirkwood–Riseman approximation for the equilibrium-averaged Oseen hydrodynamic interaction coefficient[19] yields

$$T_{jk} = 1/[(6\pi^3)^{1/2}\eta_e\langle R_{jk}^2\rangle^{1/2}] \quad (16)$$

with η_e the viscosity of the solvating medium and $\langle R_{jk}^2\rangle$ the mean-square distance between the jth and the kth beads. Assuming that η_e is constant throughout the volume occupied by the entire chain, one obtains

$$H'_{jk} = \rho_A/[(6\pi^3)^{1/2}\eta_e\langle R_{jk}^2\rangle^{1/2}] = 2^{1/2}\rho_A/[(12\pi^3)^{1/2}\eta_e b_A \times \langle R_{jk}^2/b_A^2\rangle^{1/2}] = 2^{1/2}h_A^*/\langle R_{jk}^2/b_A^2\rangle^{1/2} \quad (17)$$

The final forms of the off-diagonal elements of the symmetric $\tilde{\tilde{H}}'$ matrix, with the appropriate substitution of $\langle R_{jk}^2\rangle$ expressions (see refs 13 and 15 for details), are as follows:

If both the jth and kth beads are from the A block

$$H'_{jk} = 2^{1/2}h_A^*/|j-k|^{1/2} \quad (18a)$$

If both the jth and kth beads are from the B block

$$H'_{jk} = 2^{1/2}h_A^*/|(j-k)/(b_A^2/b_B^2)|^{1/2} \quad (18b)$$

If both the jth and kth beads are from the C block

$$H'_{jk} = 2^{1/2}h_A^*/|(j-k)/(b_A^2/b_C^2)|^{1/2} \quad (18c)$$

If the jth bead is from the A block and the kth bead is from the B block

$$H'_{jk} = 2^{1/2}h_A^*/[(N_A - j - {}^1/_2) + (k - N_A + {}^1/_2)/(b_A^2/b_B^2)]^{1/2} \quad (18d)$$

If the jth bead is from the B block and the kth bead is from the C block

$$H'_{jk} = 2^{1/2}h_A^*/[(N_A + N_B - j - {}^1/_2)/(b_A^2/b_B^2) + (k - N_A - N_B + {}^1/_2)/(b_A^2/b_C^2)]^{1/2} \quad (18e)$$

If the jth bead is from the A block and the kth bead is from the C block

$$H'_{jk} = 2^{1/2}h_A^*/[(N_A - j - {}^1/_2) + N_B/(b_A^2/b_B^2) + (k - N_A - N_B + {}^1/_2)/(b_A^2/b_C^2)]^{1/2} \quad (18f)$$

Thus, for any particular triblock copolymer model chain, once the values of the parameters N_A, N_B, N_C, b_A^2/b_B^2, b_A^2/b_C^2, ρ_A/ρ_B, ρ_A/ρ_C, and h_A^* are specified, the $\tilde{\tilde{H}}'$ matrix elements can be calculated from eqs 14a–c and 18a–f. Since the matrices $\tilde{\tilde{A}}'$ and $\tilde{\tilde{H}}'$ are symmetric and the λ'_k, the eigenvalues of $\tilde{\tilde{H}}'\cdot\tilde{\tilde{A}}'$, are distinct, the VE properties of the linear block copolymer model chain are also determined by the λ'_k.[13] The reduced intrinsic complex shear moduli predicted for the linear block copolymer model chain are given by the same expressions (eq 6) as those for a linear homopolymer model chain; the differences in the VE properties predicted for the two cases are determined solely by the differences in the relaxation time spectra. Here $\tau_k = b_A^2\rho_A/6k_BT\lambda'_k$.

(iv) $\tilde{\tilde{B}}'$ Matrix for a Linear Block Copolymer. Alternatively, the equations for the spring vectors of a linear block copolymer model chain can be separated from the equation for the center of hydrodynamic resistance in a manner similar to that described by Lodge and Wu for the linear homopolymer model chain. Namely, one can replace the $\tilde{\tilde{H}}'\cdot\tilde{\tilde{A}}'$ matrix by a $\tilde{\tilde{B}}'$ matrix; both possess the same nonzero eigenvalues but the former has the extra λ_0 (=0). The elements of the block copolymer $N \times N$ $\tilde{\tilde{B}}'$ matrix are given by (see ref 13 for details):

$$B'_{ij} = E_j(H_{ij} - H_{i,j-1} - H_{i-1,j} + H_{i-1,j-1}) \quad (19)$$

It is worth noting that, because of the ratio of the mean-square spring lengths E_j in eq 19, the block copolymer $\tilde{\tilde{B}}'$ matrix is *nonsymmetric*, in contrast to the Lodge–Wu $\tilde{\tilde{B}}$ matrix for a homopolymer model chain, which is symmetric. So, whereas in the homopolymer case the symmetry of the $\tilde{\tilde{B}}'$ matrix could be utilized to minimize computer storage requirements as well as computation time, in the block copolymer case this advantage is lost, and all N^2 elements have to be stored and calculated.

(v) $\tilde{\tilde{P}}$ Matrix for a Linear Block Copolymer. In treating the VE properties of block copolymers, one takes

into account mechanical differences of the dissimilar segments through the model parameters b_i^2 and ρ_i. To describe the flow birefringence of block copolymers one must consider not only these factors, but also the differences in segmental polarizability anisotropies of the various blocks. In this work such differences are reflected by different submolecule optical constants q_i along the triblock copolymer model chain:

$$q_i = q_A \quad \text{for } 1 \le i \le N_A - 1 \tag{20a}$$

$$q_i = (q_A + q_B)/2 \quad \text{for } i = N_A \tag{20b}$$

$$q_i = q_B \quad \text{for } N_A + 1 \le i \le N_A + N_B - 1 \tag{20c}$$

$$q_i = (q_B + q_C)/2 \quad \text{for } i = N_A + N_B \tag{20d}$$

$$q_i = q_C \quad \text{for } N_A + N_B + 1 \le i \le N \tag{20e}$$

(Note that again the solvent refractive index has been assumed to match the isotropic part of the refractive indices of all the blocks to eliminate form birefringence effects.)

A symmetric tridiagonal $(N+1) \times (N+1)$ matrix $\tilde{\tilde{P}}$ can then be constructed with elements P_{jk} given by

$$P_{0,k} = q_1\delta_{0,k} - q_1\delta_{1,k} \tag{21a}$$

$$P_{j,k} = -q_j\delta_{j-1,k} + (q_j + q_{j+1})\delta_{j,k} - q_{j+1}\delta_{j+1,k} \tag{21b}$$

$$P_{N,k} = -q_N\delta_{N-1,k} + q_N\delta_{N,k} \tag{21c}$$

where the q_j are given by eqs 20a–e and $\delta_{j,k}$ is the Kronecker δ (0 if $j \neq k$; 1 if $j = k$). Low shear rate OFB properties for the linear block copolymer model chain are then given by (see refs 14 and 15 for details)

$$[S_m]_P = [[\sum_k (\pi_k/\mu_k)\tau_k/(1 + \omega^2\tau_k^2)]^2 + [\sum_k (\pi_k/\mu_k)\omega\tau_k^2/(1 + \omega^2\tau_k^2)]^2]^{1/2} \tag{22a}$$

and

$$[\theta]_P = \tan^{-1}[-\sum_k (\pi_k/\mu_k)[\omega\tau_k^2/(1 + \omega^2\tau_k^2)]/\sum_k (\pi_k/\mu_k)[\tau_k/(1 + \omega^2\tau_k^2)]] \tag{22b}$$

where the relaxation times τ_k are related to λ'_k, the eigenvalues of the $\tilde{\tilde{H}}'\cdot\tilde{\tilde{A}}'$ matrix by $\tau_k = b_A^2\rho_A/6k_BT\lambda'_k$:

$$\pi_k = (\tilde{\alpha}_k)^T\cdot\tilde{\tilde{P}}\cdot\tilde{\alpha}_k \tag{23}$$

where $\tilde{\alpha}_k$ is the kth eigenvector of the $\tilde{\tilde{H}}'\cdot\tilde{\tilde{A}}'$ matrix; and

$$\mu_k = (\tilde{\alpha}_k)^T\cdot\tilde{\tilde{A}}'\cdot\tilde{\alpha}_k \tag{24}$$

Note that the π_k/μ_k are mode-dependent optical weighting factors that can lead to substantial differences in the frequency dependence of OFB vs VE properties; in general, the stress-optic relation $(S^* - S_e^*) = C(\eta^* - \eta_e^*)$ will not hold for block copolymer solutions. For the special case of a homopolymer

$$\tilde{\tilde{P}}\,(\text{homopolymer}) = q\tilde{\tilde{A}}\,(\text{homopolymer}) \tag{25}$$

from which

$$\pi_k\,(\text{homopolymer}) = q\mu_k\,(\text{homopolymer}) \tag{26}$$

Thus, for the special case of a homopolymer the mode-dependent optical weighting factors π_k/μ_k reduce to the mode-invariant submolecule optical constant q, and eqs 22a and b revert to eqs 7b and c, respectively. The low shear rate complex viscosity and complex mechano-optic coefficients for very dilute solutions of flexible block copolymers are still fairly simply related, although not as simply as for the homopolymer case (see eqs 8 and 9). Here the quantity (π_k/μ_k) leads to a different stress-optic coefficient for each mode.

Chart I
Calculational Flow Diagrams

I. Homopolymer: [set up half of symmetric $\tilde{\tilde{B}}$] → [solve for λ_k] → [calculate VE (eqs 6a and b) and OFB (eqs 7b and c)]

II. Block copolymer: [set up entire nonsymmetric $\tilde{\tilde{B}}'$] → [solve for λ'_k] → [calculate VE (eqs 6a and b)]

III. Block copolymer: [set up $\tilde{\tilde{H}}'$, $\tilde{\tilde{A}}'$, and $\tilde{\tilde{P}}$ separately] → [calculate the product $\tilde{\tilde{H}}'\cdot\tilde{\tilde{A}}'$] → [solve for both λ'_k and $\tilde{\alpha}_k$ for $\tilde{\tilde{H}}'\cdot\tilde{\tilde{A}}'$] → [calculate π_k and μ_k as $(\tilde{\alpha}_k)^T\cdot\tilde{\tilde{P}}\cdot\tilde{\alpha}_k$ and $(\tilde{\alpha}_k)^T\cdot\tilde{\tilde{A}}'\cdot\tilde{\alpha}_k$, respectively] → [calculate VE (eqs 6a and b); calculate OFB (eqs 22a and b)]

$$\eta^* = \frac{cRT}{M}\sum_k \frac{\tau_k}{1 + i\omega\tau_k} + \eta_e^* \tag{27}$$

and

$$S^* = \frac{cN_Aq_Ab_A^2}{M}\sum_k \left(\frac{\pi_k}{\mu_k}\right)\frac{\tau_k}{1 + i\omega\tau_k} + S_e^* \tag{28}$$

It should be emphasized that since the VE properties of a block copolymer are only dependent on the relaxation times, while the OFB properties of a block copolymer are dependent on both the relaxation times and the mode-dependent optical weighting factors, the frequency response of block copolymer OFB properties is predicted to be much more sensitive than VE properties to the precise chemical structure, including the sequences and sizes of the blocks along the copolymer chain.

C. Calculation Scheme for Block Copolymer VE and OFB Properties. The BSM for a linear triblock copolymer involves 11 parameters (N_A, N_B, N_C, h_A^*, b_A^2/b_B^2, b_A^2/b_C^2, ρ_A/ρ_B, ρ_A/ρ_C, q_A, q_B, and q_C). In contrast, for a linear homopolymer, only three variables (N, h^*, and q) need to be specified. The different computational pathways for a homopolymer and a block copolymer are contrasted in the "calculational flow diagrams" shown in Chart I.

In this work, two main Fortran programs have been written for linear triblock copolymers. The first one, WMAN, performs the calculations shown as pathway II, and therefore is only applicable for VE predictions; an upper limit for N of ~243 was reached with a Harris /7 computer. The second program, WMANVB, performs the calculations shown as pathway III and therefore is applicable for both VE and OFB predictions; an upper limit for N of ~190 was reached with the Harris /7 computer. Recently, calculations with WMANVB have reached an upper limit for

$N \approx 3000$ with a MASSCOMP 500. Both programs utilize the EISPACK library routine, which solves for both the eigenvalues and eigenvectors for general matrices.

III. Results

A. Analytic Expressions for π_k/μ_k for Free-Draining, Mechanically Uniform Block Copolymers. There exist no general closed-form analytic solutions for the exact λ_k and $\tilde{\alpha}_k$ (and thus also π_k/μ_k) for a BSM chain with $N > 4$ unless two conditions are met: (1) the chain is mechanically uniform (there is only one mean-square spring length and one bead drag coefficient); (2) there is no hydrodynamic interaction between the beads (i.e., $h^* = 0$, free-draining limit). If these two conditions are satisfied, exact analytical solutions for λ_k and $\alpha_k(j)$ (the jth element of the kth eigenvector) were found by Rouse[5] to be

$$\lambda_k = \mu_k = 4 \sin^2 (\beta/2) \qquad k = 0, 1, 2, ..., N \tag{29a}$$

$$\alpha_k(j) = [2/(N+1)]^{1/2}(1/2)^{1/2} \qquad k = 0 \tag{29b}$$

$$\alpha_k(j) = [2/(N+1)]^{1/2} \cos [\beta(j + 1/2)] \qquad k = 1, 2, 3, ..., N$$

where $\beta = k\pi/(N+1)$. One can then set up the $\tilde{\tilde{P}}$ matrix for a specific block copolymer as described earlier and derive an expression for π_k by carrying out the scalar dot product $(\tilde{\alpha}_k)^T \cdot \tilde{\tilde{P}} \cdot \tilde{\alpha}_k$.

(i) Free-Draining, Mechanically Uniform Diblock. The expression thus derived for a free-draining mechanically uniform diblock (see ref 15 for details) is

$$\pi_k/\mu_k = [1/(N+1)][(q_A + q_B)[N - N_A - [\cos [(N - N_A + 1)\beta] \sin [(N - N_A)\beta]/\sin \beta]] + q_A[2N_A - N - [\sin [(2N_A - N)\beta] \cos (k\pi)/\sin \beta]]] \tag{30}$$

The approximation $q_{AB} = q_A$ was used for ease of derivation (recall that the model calls for $q_{AB} = (q_A + q_B)/2$). Therefore, eq 30 is only applicable for N large, and $(N_A q_A + N_B q_B)$ not approaching zero. At present, accurate calculations for N small, and/or $(N_A q_A + N_B q_B)$ approaching zero, can only be obtained with the WMANVB program.

Although it is well-established that the free-draining ($h^* = 0$) limit does not describe flexible chains in dilute solution, some interesting features of block copolymer dynamics can be deduced from eq 30.

(1) When $N = 2N_A$ (i.e., $N_B = N_A + 1$ and N is even), eq 30 reduces to

$$\pi_k/\mu_k = (q_A + q_B)/2 \tag{31}$$

The condition $N_B = N_A + 1$ compensates for the approximation $q_{AB} = q_A$ in the derivation of eq 30. Significantly, eq 31 holds for WMANVB calculations for any N and h^* in the mechanically uniform chain limit as soon as the two blocks are identical in size (i.e., $N_A = N_B$, and N is odd. Note that for a symmetric diblock copolymer, N must be odd). Equation 31 means that the weighting factors are *independent* of the mode index k, and the OFB properties are identical with those for a homopolymer with a stress-optic coefficient equal to the average of those for the two blocks. Also, when q_A is equal to q_B in magnitude but opposite in sign, all the optical weighting factors become zero. This is intuitively reasonable, as the center of hydrodynamic resistance is located at the center of the model chain, and thus the birefringence originating from one half of the chain is exactly canceled by that from the other half.

(2) There is a symmetry in the π_k/μ_k spectrum with respect to $k = (N+1)/2$, N odd, for free-draining mechanically uniform diblocks. This can be seen by substituting $N - (k-1)$ in place of k in eq 30. Again, WMANVB calculations show that this is a fundamental property of the free-draining mechanically uniform model chain regardless of the size of N, and for N odd or even. In addition, WMANVB calculations have shown the following relationship for the central mode ($k = (N+1)/2$, N odd):

$$\pi_{(N+1)/2}/\mu_{(N+1)/2} = (N_A q_A + N_B q_B)/(N+1) \tag{32}$$

(ii) Free-Draining Mechanically Uniform Symmetric Triblock. The triblock problem is mathematically more complicated than the diblock problem since the number of parameters changes from four (N_A, N_B, q_A, q_B) to six ($N_A, N_B, N_C, q_A, q_B, q_C$). However, when the two end blocks are identical both in size and in optical constant ($N_A = N_C$ and $q_A = q_C$), analytical expressions can be derived:[14]

$$\pi_k/\mu_k = [1/(N+1)][q_A[2N_A + 1 - [\sin [(2N_A+1)\beta]/\sin \beta]] + q_B[N_B - 1 - (-1)^k[\sin [(N_B-1)\beta]/\sin \beta]]] \tag{33}$$

In obtaining eq 33, the approximations $q_{AB} = q_{BC} = q_A$ are used for the junction submolecules in setting up the $\tilde{\tilde{P}}$ matrix. Thus, as in the diblock case above, this relation applies only for N large and $(N_A q_A + N_B q_B + N_C q_C)$ not approaching zero. Listed below are some interesting features deduced from this result, together with WMANVB calculations.

(1) There is a symmetry in the π_k/μ_k spectrum with respect to $k = (N+1)/2$, N even or odd, for these special case symmetric triblocks as well, as shown by WMANVB calculations.

(2) WMANVB calculations have established the following relationship for the central mode ($k = (N+1)/2$, N odd):

$$\pi_{(N+1)/2}/\mu_{(N+1)/2} = [2N_A q_A + N_B q_B]/(N+1) \tag{34}$$

Interestingly, eq 32 (for an AB diblock) and eq 34 (for an ABA symmetric triblock) are equivalent in the sense that

$$\pi_{(N+1)/2}/\mu_{(N+1)/2} = [(\text{total no. of } A\text{-type beads})q_A + (\text{total no. of } B\text{-type beads})q_B]/(\text{total no. of beads in the chain}) \tag{35}$$

Extensive WMANVB calculations indicate that eq 35 is not restricted to diblocks and symmetric triblocks alone, but is applicable for any spatial distribution of the components along the model chain and is an inherent property of a free-draining mechanically uniform model chain. A comparison of the π_k/μ_k spectrum of an AB diblock with that of an ABA symmetric triblock with the same component compositions reveals that the biggest differences are at the two ends of the spectra; the differences decrease toward zero as k approaches $(N+1)/2$ from either end.

B. Contribution from an Arbitrary Chain Segment to the Total OFB of a Homopolymer. To understand the predicted OFB properties for block copolymers with increasing degrees of complexity, it is helpful as a first step to understand the contribution from any segment along the chain to the total OFB of a homopolymer. The WMANVB program can be used to examine the contribution to the predicted OFB properties that originates from any desired site in the BSM chain; the segment whose contribution is being examined is selected by manipulating the $\tilde{\tilde{P}}$ matrix to make the rest of the chain optically

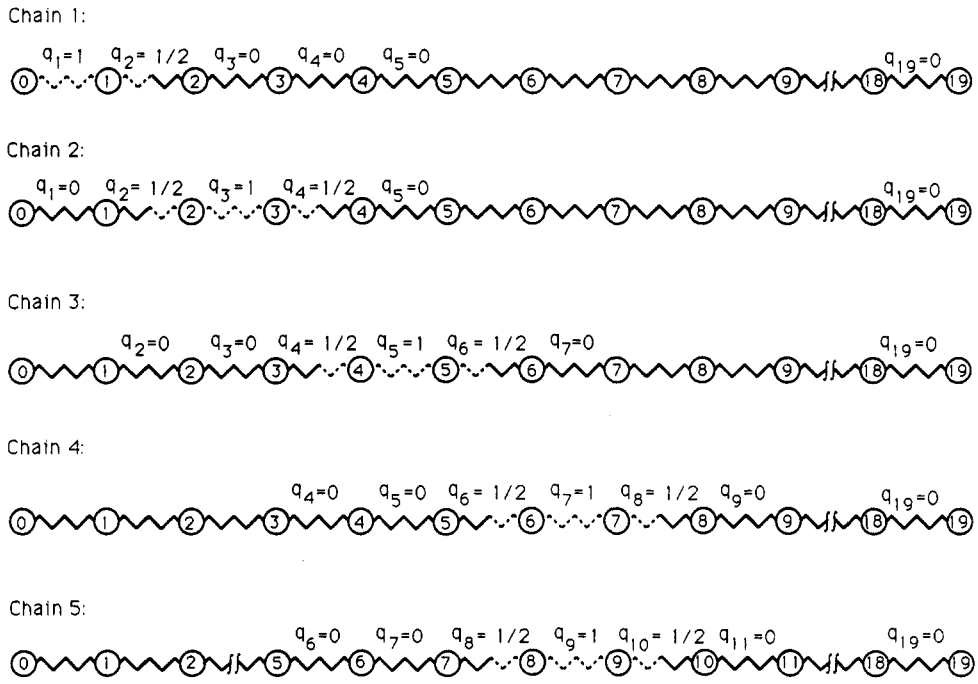

Figure 2. Illustration of a series of mechanically uniform (homopolymer) model chains with selected anisotropic segments. Only the dotted segments are anisotropic.

isotropic. Figure 2 illustrates a series of calculations that have been performed; each of the five chains is made up of 20 beads and 19 springs with identical spring constants and drag coefficients. However, only the dotted segment of each chain is assigned a nonzero optical constant q (normalized to 1); therefore, only the dotted segment in each chain is optically anisotropic and can contribute any birefringence; the dotted segment is in a different location for each of the five chains.

Figure 3 shows the viscoelastic results for these five chains for $h^* = 0$. They are identical with Rouse chain results for $N = 19$. However, these five chains produce drastically different OFB results, as shown in Figure 4. For comparison, the dashed lines show the results for a "total" chain with $q = 1$ for all 19 submolecules. The results for each chain are presented as log $[(S_m)_j/(S_{mo})_{TOT}]_P$ and $(-[\theta-\theta_o]_{Pj})$ vs log $(\omega\tau_1)$, in which $(S_{mo})_{TOT}$ is the magnitude of the mechano-optic coefficient for the "total" chain in the low-frequency limit.

The OFB properties in the low- and high-frequency limits for these five chains are tabulated below:

	chain 1	chain 2	chain 3	chain 4	chain 5
$[(S_{mo})_j/(S_{mo})_{TOT}]_P$	0.0278	0.0759	0.112	0.136	0.148
$\left[\left[\frac{(S_m)_j}{(S_m)_{TOT}}\right]_P\right]_{\omega\to\infty}$	0.0789	0.105	0.105	0.105	0.105

The most interesting and important observations from these calculations are the following:

(1) In the low-frequency limit ($\omega\tau_1 < 1$) the chain center contributes a much larger birefringence than the chain end; the birefringence of chain 5 is more than 5 times that of chain 1 in this limit. This positional dependence becomes smaller as frequency increases, and finally, at high frequency ($\omega\tau_N > 1$) they contribute equally. At the high-frequency limit the birefringence contributed is proportional to the length of the segment. This can be seen from the result that $([(S_m)_{TOT}/(S_m)_j]_P)_{\omega\to\infty} = 9.5 = 19/2$ for chains 2–5 and $([(S_m)_{TOT}/(S_m)_1]_P)_{\omega\to\infty} = 12.67 = 19/1.5$. The "total" chain has 19 anisotropic submolecules while chains 2–5 each have 2 anisotropic submolecules and chain 1 has 1.5 anisotropic submolecules.

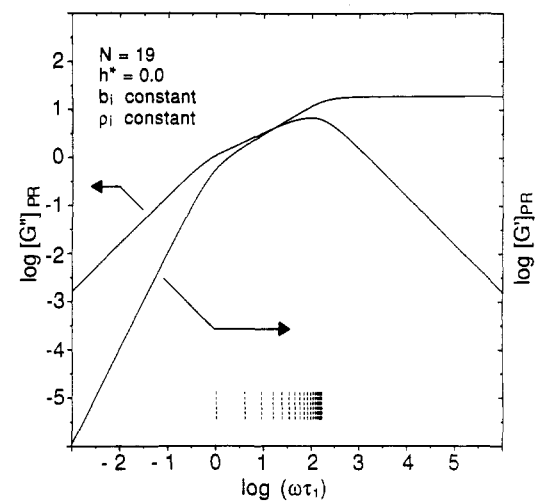

Figure 3. Predicted VE properties for model chains illustrated in Figure 2, $h^* = 0$.

(2) The frequency dependence of the phase angle of the birefringence relative to the shear rate $(-[\theta - \theta_o]_{Pj})$ for these chains is also very interesting. The phase-angle curve for chain 5 rises very quickly initially and then actually dips slightly before it rises to the 90° high-frequency limit. Therefore, it lies above the "total" curve over most of the frequency range and has a characteristic bump at around log $\omega\tau_1 = 0.5$. In contrast, the phase-angle curve for chain 1 is substantially depressed below the "total" curve. Both the magnitude and relative phase of the birefringence for each chain reflect the peculiar pattern of each set of optical weighting factors. The six sets of π_k/μ_k for chains "total" and 1–5, each for $h^* = 0$, are shown respectively in Figure 5.

The π_k/μ_k for chain "total" are all equal to 1, as must be the case (recall that the nonzero q is normalized to 1). Chain 1 starts out with a very small π_1/μ_1, and π_k/μ_k

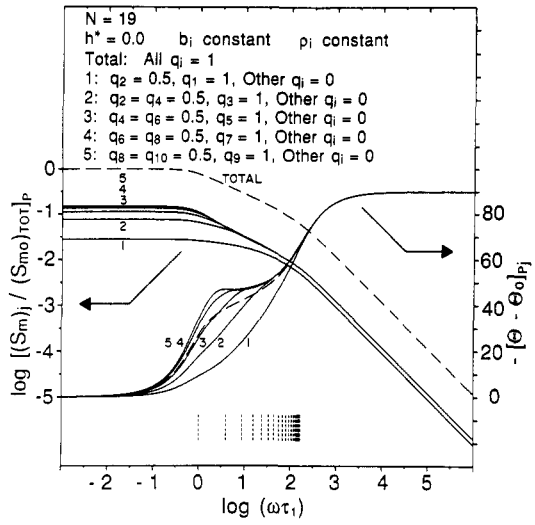

Figure 4. Predicted OFB properties for model chains illustrated in Figure 2, $h^* = 0$.

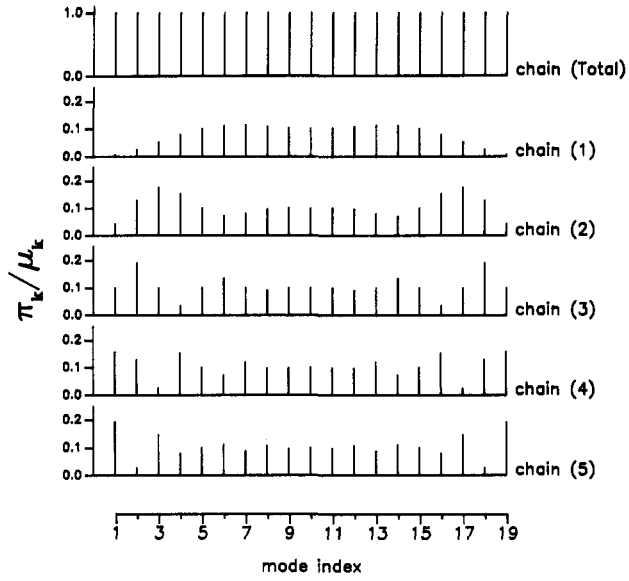

Figure 5. Calculated optical weighting factors (π_k/μ_k) for model chains illustrated in Figure 2, $h^* = 0$, corresponding to results shown in Figure 4.

steadily increases through the first few modes. This is why the phase-angle curve for chain 1 is depressed below the "total" curve. Chain 3 has a characteristically large π_2/μ_2, which explains why its phase-angle curve goes above the "total" curve at intermediate frequencies; chain 3 also has a relatively large π_6/μ_6. Chain 5 shows a characteristic pattern of large π_1/μ_1 and π_3/μ_3, and small π_2/μ_2 and π_4/μ_4. This is responsible for the bump in the phase-angle curve between $\omega\tau_1 = 1$ and $\omega\tau_2 = 1$.

It is difficult to understand, even qualitatively, the mode dependence of any π_k/μ_k spectrum. It has been found in this study that it is helpful to visualize each normal mode of motion of the bead–spring model chain as being similar to that of a damped freely vibrating elastic string with free ends. Empirically it seems evident that when a selected anisotropic segment is located at a motional envelope nodal point, it is highly stretched and will contribute strongly to the birefringence through the optical weighting factor for that particular mode; the opposite applies for a selected anisotropic segment located at an envelope maximum point.

(3) It is also found that the following relationship holds at any frequency:

$$(S_P^*)_{TOT} = 2(S_{P1}^* + S_{P2}^* + S_{P3}^* + S_{P4}^* + S_{P5}^*) \qquad (36)$$

This indicates that the polarizability tensor for every submolecule in the bead–spring model has the same orientation of the principal axes, and the OFB contributions can be separately calculated and added vectorially at each frequency in the complex plane to obtain the "total" birefringence at each frequency (also observed to be the case for nonzero h^* and mechanically nonuniform chain conditions). One ramification of this is that even though the WMANVB program is written for a triblock (naturally also applicable for a diblock), it can also be used to calculate OFB properties for a many-block copolymer provided that the chain is mechanically uniform; of course, multiple calculations have to be performed and summed vectorially.

Results of calculations of the frequency dependence of the birefringence for the same five model chains but for $h^* = 0.25$ (nonfree-draining limit) are very similar to what is shown in Figure 4. The relaxation times are now more closely spaced, resulting in a reduced relaxation time spectrum breadth, and the low-frequency OFB of chains 1 and 2 in particular has increased; for chain 1 the increase is approximately a factor of 2. The influence of large h^* on π_k/μ_k spectra is small. However, for nonzero h^* the symmetry of π_k/μ_k about $k = (N+1)/2$ is slightly distorted. Nonetheless, eq 36 is still found to hold at any frequency, again showing that the OFB contribution from every submolecule in the model, regardless of the degree of hydrodynamic interaction, can be separately calculated and added vectorially in the complex plane to obtain the "total" chain birefringence at each frequency.

To help in interpreting predicted OFB and VE properties, Figure 3 and most subsequent figures also show line spectra (toward bottom of figure) of the sets of discrete relaxation times. Each of the N vertical lines corresponds to a relaxation time for a normal mode of the bead–spring chain. The lines are drawn at points along the reduced frequency ($\omega\tau_1$) axis where $\omega\tau_k = 1$, so that $\omega\tau_1 = \tau_1/\tau_k = \lambda_k/\lambda_1$. The spacing between adjacent relaxation times usually decreases with increasing mode number.

Also, several subsequent figures show OFB predictions calculated for $h^* = 0$. Results for $0 < h^* \leq 0.25$ are again qualitatively the same, but show somewhat smaller differences between the various cases considered than are seen for $h^* = 0$. Thus the $h^* = 0$ results are included here for visual clarity.

C. Predicted Frequency Dependence of Characteristic OFB Properties for Block Copolymers That Have Both Positively and Negatively Birefringent Components: Mechanically Uniform Chain Limit. Styrene–diene block copolymers should be particularly sensitive to OFB studies because one component (polystyrene) has a negative intrinsic segmental anisotropy while the other component (either polybutadiene or polyisoprene) has a positive one. For cases where the optical nonuniformity in a block copolymer chain is due to q with different magnitudes but equal sign, the predicted frequency dependence of θ_P curves remains either above or below that for an optically uniform chain (homopolymer) of the same N, and in the same quadrant; (i.e., for positive birefringences, 0° to −90°, and for negative birefringences, −180° to −270°). However, for cases where the two components are different both in the magnitude and in the sign of q, the resultant phase-angle curves can exhibit striking frequency dependences and frequently do not remain in one quadrant, as will be shown below. A variety of curve shapes can be produced by using different

combinations of model parameter values. Here the emphasis is to illustrate and explain qualitatively some important classes of behavior.

(i) Theoretical Predictions for *A–B–A* Symmetric Triblocks. Consider a case where the total amount of A is ≈30% and the total amount of B is ≈70% of the chain, q_A is negative and q_B is positive, and $|q_A/q_B| > 1$; this might correspond to PS–PB–PS and PS–PI–PS triblocks examined experimentally.[12,15,18] To gain more perspective, we will first look separately at the normalized contributions predicted for the two A blocks at the ends and the B block at the center. Consider first two model chains, each consisting of 20 beads and 19 springs. Each chain is mechanically uniform throughout, the two chains are mechanically identical, and q_A and q_B have the same sign. In chain 1, the two A end blocks are each 3.5 submolecules in size, with $q_A = 1$, while the 12 submolecules of the center B block have $q_B = 0$. In chain 2, $q_A = 0$ and $q_B = 1$. Figure 6 shows the calculated OFB results for $h^* = 0$. Note that the OFB magnitude curves have been normalized by dividing by the low-frequency limiting value $(S_{mo})_{REF}$ for a reference homopolymer chain with $N = 19$, $h^* = 0$, ρ_i constant, and $q_i = +1$; this same reference chain S_{mo} has been employed to normalize several other figures as well, to illustrate relative changes in OFB levels as the block copolymer structures are varied. The most important results are that the ratio $(S_m)_B/(S_m)_A = 3.819$ as $\omega\tau_1 \to 0$ and 1.714 (=12/7) as $\omega\tau_1 \to \infty$. As expected, because of its strategic central position, the normalized B block dominates the OFB at the low-frequency limit. In the high-frequency limit, however, the level of the respective contributions solely reflects the number of submolecules (the block size) regardless of position. The effect of changing the magnitude of the nonzero q_i is to shift the entire magnitude curve vertically, with no change in θ_P. In this example, $\theta_{P_0} = 0°$ for both chains. However, for a chain with negative q, $\theta_{P_0} = -180°$; this difference is concealed when the plotted quantity is $-[\theta - \theta_0]_P$.

When the two components are both present with q_A negative and q_B positive, the resultant birefringence will be distinctively different for three different ranges of q_A/q_B, which can be deduced from the values given above; recall that these are for $h^* = 0$.

(1) $0 > q_A/q_B > -1.714$. Within this range, the sign of the net birefringence will be positive in both low- and high-frequency limits.

(2) $-1.714 > q_A/q_B > -3.819$. The net birefringence sign will be positive in the low-frequency limit but negative in the high-frequency limit.

(3) $-3.819 > q_A/q_B$. The net birefringence sign will be negative in both the low- and high-frequency limits.

We will illustrate these three classes of characteristic curve shapes with three case studies.

Case 1: q_A $(=q_C) = -1.5$, $q_B = 1.0$; $h^* = 0$. In Figure 7, the OFB properties resulting from only the negatively birefringent (A blocks) or positively birefringent (B block) components are calculated and shown separately as curves 1 and 2. These illustrate why the OFB for the entire triblock (both contributions present), calculated and shown as curve 3, exhibits such an unusual frequency dependence. The net triblock magnitude (curve 3) starts out fairly high, drops steeply from $\omega\tau_1 \simeq 1$ to 20, and then shows an inflection region before it continues into a high-frequency regime (negative first power slope). The entire triblock θ_P curve (curve 3) rises steeply at around $\omega\tau_1 \simeq 1$, reaches a maximum, and displays a minimum before it rises again to the high-frequency limit of −90° (for this case $\theta_{P_0} = 0°$). Note that at all frequencies the triblock phase-angle curve

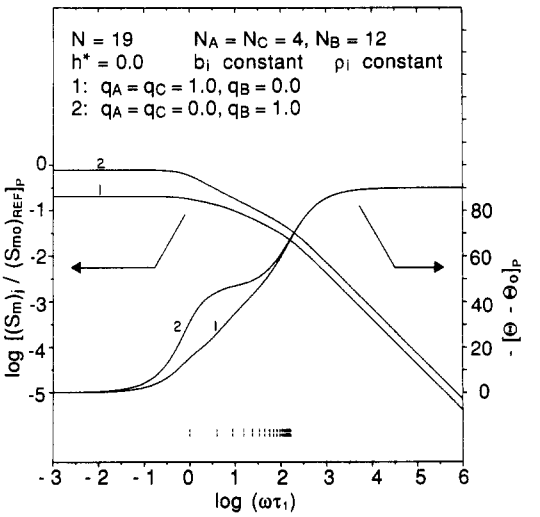

Figure 6. Predicted OFB contributions from two end A blocks (curve 1) and central B block (curve 2) of an A–B–A symmetric triblock; mechanically uniform chain limit. Magnitude curves normalized by dividing by S_{mo} for a reference homopolymer chain with $N = 19$, $h^* = 0$, ρ_i constant, b_i constant, and $q_i = +1$.

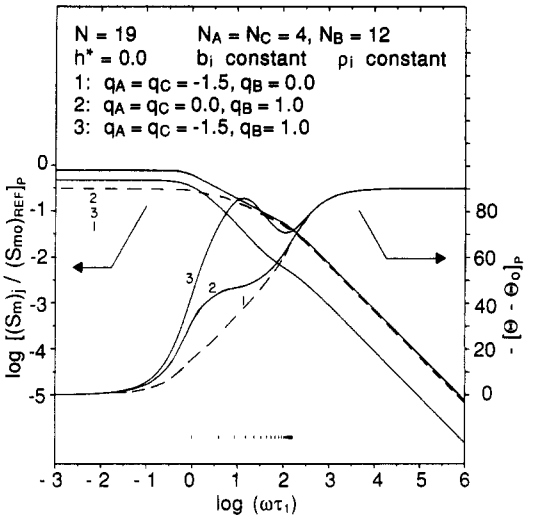

Figure 7. Predicted OFB properties for an A–B–A symmetric triblock (curve 3), with contributions from two end A blocks (curve 1) and central B block (curve 2) also shown; mechanically uniform chain limit with $q_A/q_B = -1.5$. Magnitude curves normalized as in Figure 6.

is above that for a mechanically equivalent but optically uniform model chain (chain "total" of Figure 4); this is a very important feature characteristic of mechanically uniform model chains.

All styrene–diene block copolymers studied experimentally (18–40.3% PS) show local maxima and minima in θ_P.[12,15,18] However, poor theoretical fits to the data were obtained through the use of eqs 30 and 33 in all of the following respects: the location, width, and height of the data θ_P peak and, most notably, the depth of the valley. In fact, some experimentally observed θ_P valleys even drop below 0°. The fact that so far the block copolymer model chain has been treated as being mechanically uniform is responsible for the theoretically predicted θ_P valley remaining above approximately −50° (always above the curve for a homopolymer model chain with the same N), because the $[\theta - \theta_0]_P$ curves of both the positively and negatively birefringent components (curves 2 and 1, respectively, in Figure 7) have merged together before $\omega\tau_N \simeq 1$. Note, however, that $\theta_{P_0} = -180°$ for curve 1 and $\theta_{P_0} = 0°$ for curve 2. We will see in a later subsection how the

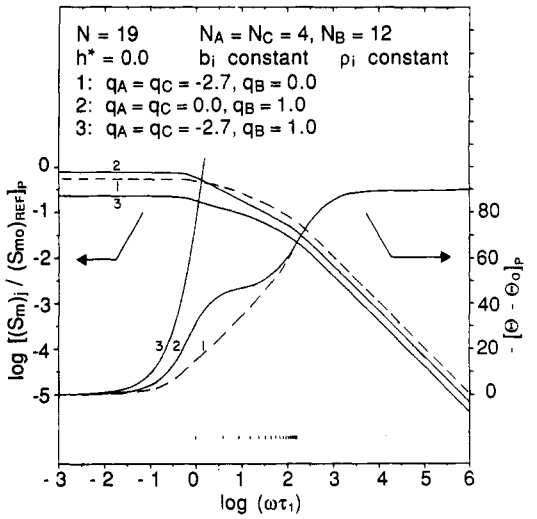

Figure 8. Predicted OFB properties for an *A–B–A* symmetric triblock (curve 3), with contributions from two end *A* blocks (curve 1) and central *B* block (curve 2) also shown; mechanically uniform chain limit with $q_A/q_B = -2.7$. Magnitude curves normalized as in Figure 6.

predicted behavior changes markedly when the blocks are allowed to be mechanically different by assigning different bead drag coefficients ($\rho_A \neq \rho_B$).

Case 2: q_A ($=q_C$) $= -2.7$, $q_B = 1.0$; $h^* = 0$. The results for this case are shown in Figure 8. In this case, the triblock birefringence (curve 3) is still positive in the low-frequency limit. However, the triblock birefringence in the high-frequency limit is negative, since $(N_A - {}^1/_2)q_A + (N_C - {}^1/_2)q_A = -18.9$ while $(N_B)q_B = +12$. The triblock θ_P (curve 3) starts out at 0° in the low-frequency limit, rises very rapidly around $\omega\tau_1 \simeq 1$, and with essentially the same steep slope, passes through the fourth and third quadrants into the second quadrant, leveling off somewhere around −220°, followed by a rapid approach to the −270° high-frequency limit at frequencies where $\omega\tau_N \simeq 1$ (in the figure, $-[\theta - \theta_0]_P$ above 90° is not shown). Also in Figure 8, the OFB properties resulting from the negatively birefringent (*A* blocks) or positively birefringent (*B* block) components are separately calculated and shown as curves 1 and 2; these aid in understanding where the net birefringence of the triblock changes sign. As in Figure 7, however, curves 1 and 2 merge in the high- and low-frequency limits only because θ_{P_0} has been subtracted.

Case 3: q_A ($=q_C$) $= -3.9$; $q_B = 1.0$; $h^* = 0$. The results for this case are shown in Figure 9. In this case, the negative birefringence due to the end *A* blocks, calculated and shown separately as curve 1, is slightly bigger than the positive birefringence due to the central *B* block, calculated and shown as curve 2, even in the low-frequency limit. Since the magnitude of the positively birefringent component drops more rapidly, and its θ_P curve rises more rapidly than that for the negatively birefringent component near $\omega\tau_1 \simeq 1$, a unique total triblock curve is obtained, which is shown as curve 3. The triblock magnitude curve has a broad hump. The triblock phase-angle curve drops into the third quadrant (−90° to −180°) before it rises steeply back into the second quadrant (−180° to −270°) at frequencies where $\omega\tau_1 \simeq 3$, eventually going to the −270° high-frequency limit; thus a low-frequency minimum in the θ_P curve has developed. Again, it should be noted that curves 1 and 2 would lie in different quadrants if θ_{P_0} were not subtracted.

(ii) Effect of Nonzero h^* (Mechanically Uniform Chain Limit). In subsection B, it was briefly pointed out that the inclusion of nonzero hydrodynamic interaction

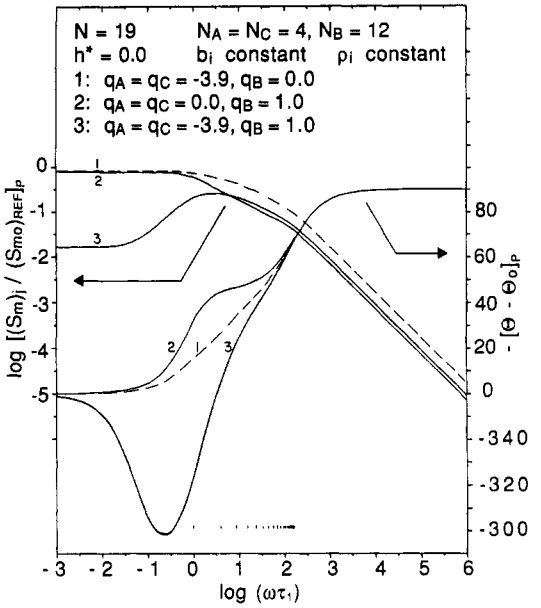

Figure 9. Predicted OFB properties for an *A–B–A* symmetric triblock (curve 3), with contributions from two end *A* blocks (curve 1) and central *B* block (curve 2) also shown; mechanically uniform chain limit with $q_A/q_B = -3.9$. Magnitude curves normalized as in Figure 6.

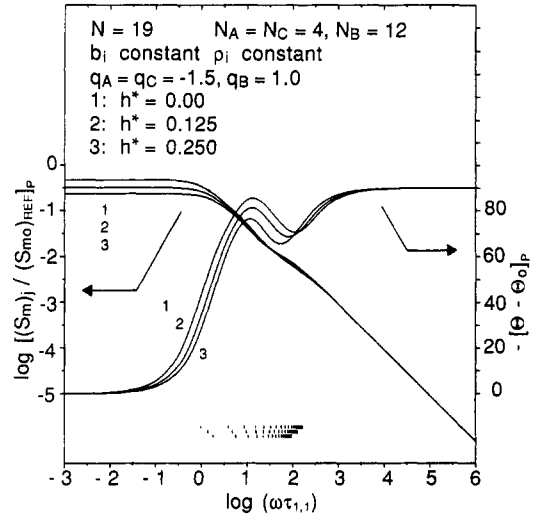

Figure 10. Effect of varying h^* on predicted OFB properties for an *A–B–A* symmetric triblock copolymer. Magnitude curves normalized as in Figure 6. $\tau_{1,1}$ is longest relaxation time for chain 1.

(even for h^* as high as 0.25) changes only slightly the characteristic optical weighting factor spectrum for any selected anisotropic segment of a homopolymer. Therefore, it can be expected that in the mechanically uniform chain limit the OFB properties for any model block copolymer should depend only weakly on h^*; a "narrowing" effect is of course expected for increasingly higher h^* because of the decreasing relaxation time spacings. For demonstrative purposes, Figure 10 shows the calculated OFB properties for a model symmetric triblock for different values of h^*. As can be seen, the θ_P peak narrows, but retains an otherwise nearly identical shape, as h^* increases. Both the θ_P peak height and valley are lowered as h^* is increased; in each case, the block copolymer θ_P curve remains above that of an optically uniform model chain with the same N and h^*. Note that the relaxation times are again indicated at the bottom of the plot.

(iii) Theoretical Predictions for *A–B* Diblocks and Comparison with Composition-Matched *A–B–A*

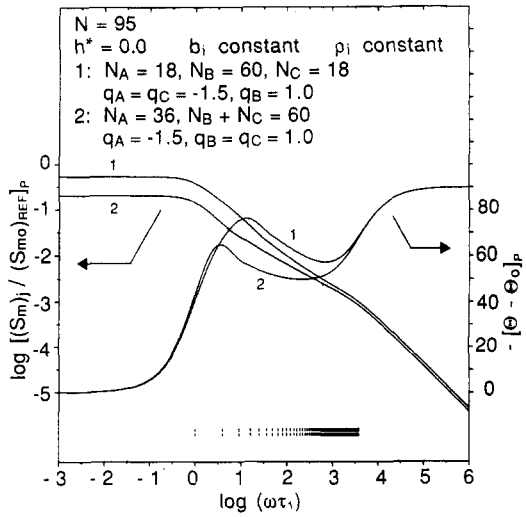

Figure 11. Comparison of predicted OFB properties for an A–B diblock and a composition-matched A–B–A triblock copolymer. Magnitude curves normalized as in Figure 6.

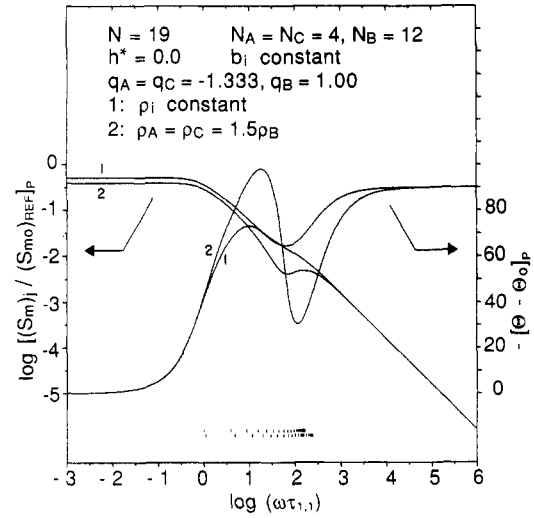

Figure 12. Comparison of predicted OFB properties for a mechanically uniform triblock (curve 1) with those for a mechanically nonuniform but otherwise identical triblock (curve 2). Magnitude curves normalized as in Figure 6.

Symmetric Triblocks. From the earlier discussions it is clear that the OFB characteristics of a diblock are distinct from those of a composition-matched triblock; here we will examine calculations that better illustrate the differences between the two. Calculations have been performed for an A–B–A model symmetric triblock with $N_A = N_C = 18$, $N_B = 60$, $b_A^2 = b_B^2 = b_C^2$, $\rho_A = \rho_B = \rho_C$, $q_A = q_C = -1.5$, $q_B = +1.0$ and a composition-matching model diblock of $N_A = 36$, $N_B + N_C = 60$, $b_A^2 = b_B^2 = b_C^2$ (and identical with those of the triblock), $\rho_A = \rho_B = \rho_C$ (and identical with those of the triblock), $q_A = -1.5$, $q_B = q_C = +1.0$. The predicted VE properties for the two chains are identical. Figure 11 compares the predicted OFB properties for the triblock (curve 1) to those for the diblock (curve 2), both for $h^* = 0$. As expected, the diblock has a much lower low-frequency birefringence than that of the triblock. However, in the high-frequency limit, the birefringence of the diblock is almost the same as that of the triblock. The comparison of the θ_P curves is even more revealing. The triblock θ_P peak attains a broader and skewed shape, while the diblock θ_P peak attains a narrower and more symmetric shape. The triblock θ_P peak height is higher and shifted more to higher frequencies in comparison to the diblock.

D. Predicted Frequency Dependence of Characteristic OFB Properties for Block Copolymers That Have Both Positively and Negatively Birefringent Components: Mechanically Nonuniform Chains. Up to this point only block copolymers that are mechanically simple (i.e., $\rho_A = \rho_B = \rho_C$; $b_A = b_B = b_C$) have been considered; here the treatment is made more realistic by considering the blocks to have different mechanical properties. Here we will again focus attention on block copolymers such as those composed of styrene and diene. Some reasonable preliminary assumptions employed are as follows: approximately equal equilibrium end-to-end length for both types of submolecules, and a larger frictional constant for a polystyrene submolecule than a polydiene submolecule. The rest of the paper deals with the examination of some characteristic VE and OFB predictions for such mechanically nonuniform model chains.

(i) Symmetric Triblock. Consider two small symmetric triblock model chains (1 and 2) each with $N_A = N_C = 4$ and $N_B = 12$; both chains have been assigned the same optical parameter values of $q_A = q_C = -1.333$ and $q_B = +1.0$. All mean-square spring lengths in the two chains are identical. The only difference is that chain 1 has a uniform bead drag coefficient while chain 2 has nonuniform bead drag coefficients ($\rho_A = \rho_C = 1.5\rho_B$) with $(\rho_A)_{\text{chain 1}}$ set equal to $(\rho_A)_{\text{chain 2}}$. Therefore, comparison of the results for chain 2 with those for chain 1 will reveal features that are characteristic of the mechanically nonuniform model chain conditions.

The VE predictions for the two chains ($h^* = 0$) are nearly the same. Since in chain 2 the central 12 beads (of the B block) have the lower drag coefficient, $(\tau_1)_{\text{chain 2}} < (\tau_1)_{\text{chain 1}}$ by ~20%. Also, the relaxation time spectral widths differ by ~35%, and the spectrum of chain 2 exhibits a break between modes 14 and 15. Thus $(\tau_1/\tau_{19})_{\text{chain 2}} = 217.4 > (\tau_1/\tau_{19})_{\text{chain 1}} = 161.4$. Although the two chains have differences in their relaxation time spectra, the differences are relatively small; the predicted frequency dependences for the VE properties for the two are also very similar.[15]

On the other hand, the predicted frequency dependences of the OFB properties for the two chains, shown in Figure 12, are remarkably different. The curve shapes for the mechanically uniform chain (chain 1) have previously been discussed. When the chain is made slightly nonuniform (chain 2), however, changes in the predicted OFB properties are unexpectedly large. It is clear that changes in the relaxation times per se have a relatively minor effect, while the major effects are caused by changes in the optical weighting factors; these are compared graphically in Figure 13.

The structure of the π_k/μ_k spectra makes their comparison somewhat complex. However, a careful comparison of each π_k/μ_k for chain 2 with that for chain 1 throughout the spectrum reveals some trends that are important in the interpretation of the OFB results. For the first 14 modes, the π_k/μ_k for chain 2 appear to have increasing contributions from the higher drag coefficient A-type submolecule (recall that q_A is negative and q_B is positive), although in a quasi-sinusoidal manner, with increasing k; the pattern is such that π_{12}/μ_{12} and π_{13}/μ_{13} have particularly large negative values. However, a different pattern develops for $k \geq 15$ for chain 2. These last five π_k/μ_k take on monotonically increasing contributions from the lower drag coefficient B-type submolecules, with increasing k; π_{19}/μ_{19} for chain 2 is +0.9844, almost equal to the value of q_B ($q_B = +1.0$). It is of interest to note that these last five modes of chain 2 belong to an apparent "B" fraction of the relaxation time spectrum and

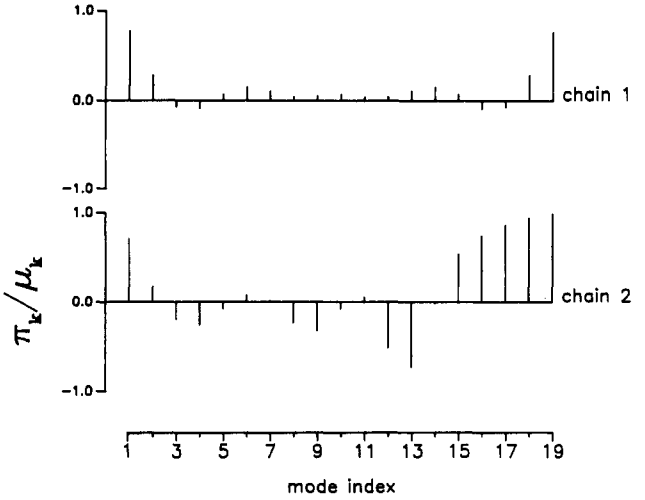

Figure 13. Comparison of the π_k/μ_k spectrum for a mechanically uniform triblock (chain 1) with that for a mechanically nonuniform but otherwise identical triblock (chain 2), corresponding to results shown in Figure 12.

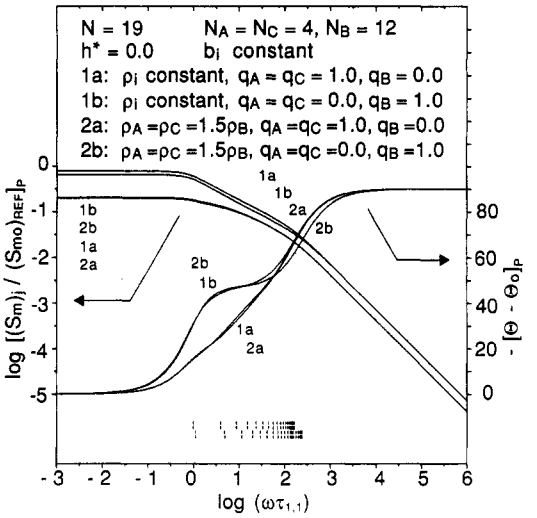

Figure 14. Comparison of predicted OFB contributions from two end A blocks (curve 1a) and central B block (curve 1b) of a mechanically uniform A–B–A symmetric triblock with those of a mechanically nonuniform but otherwise identical triblock (curves 2a and 2b). Magnitude curves normalized as in Figure 6.

are the ones that are somewhat separated from the rest of the spectrum.

Since it is difficult to interpret the trends exhibited by the π_k/μ_k spectrum for chain 2 and chain 1, it is helpful to look separately at the normalized OFB contributions ($q = 1$) from the A and B spatial components in each chain. The normalized OFB contributions from the (higher drag coefficient) A component and the (lower drag coefficient) B component of chain 2 shown in Figure 12 have been calculated separately (with WMANVB); these results are plotted in Figure 14, and labeled as 2a and 2b, respectively. Likewise, the normalized OFB contributions from the equal drag coefficient A and B components of chain 1 in Figure 12 have been calculated separately (with WMANVB) and plotted in Figure 14, where they are labeled as 1a and 1b. In Figures 12 and 14, $\tau_{1,1}$ is the longest relaxation time of chain 1 and $(S_{mo})_{REF}$ is the steady-flow mechano-optic coefficient of a chain that is mechanically equivalent to chain 1 but has all q_i normalized to be 1. The π_k/μ_k spectra corresponding to curves for 1a, 1b, 2a, and 2b are plotted in Figure 15.

As can be seen in Figure 15, for $k < 14$, the higher ρ A blocks in chain 2 (2a) increase their normalized OFB

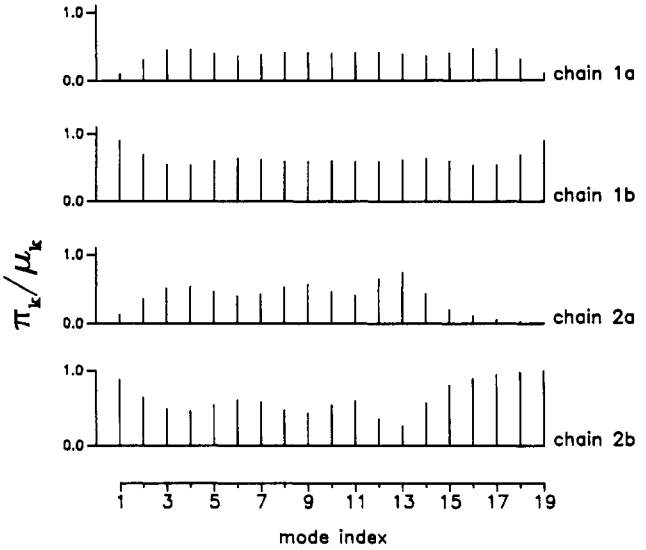

Figure 15. Comparison of the π_k/μ_k spectra for the chains in Figure 14.

contribution, although in a quasi-sinusoidal manner, with increasing k as compared to 1a. However, for $k \geq 15$, the higher ρ A blocks decrease their normalized OFB contribution monotonically as though they become increasingly more inactive; π_{19}/μ_{19} for 2a drops to 0.006 60, as compared to 0.099 76 for 1a. Exactly opposite behavior is exhibited by the lower ρ B block. Evidently, as the last five modes take on disproportionally large characteristics of the lower ρ B-type submolecules in their relaxation times, they also have disproportionally large normalized OFB contributions from these submolecules as well.

Some of the more important observations from Figure 14 are listed below.

(1) $[S_{m\infty}]_P(2a) = [S_{m\infty}]_P(1a)$, and $[S_{m\infty}]_P(2b) = [S_{m\infty}]_P(1b)$. This and other calculations demonstrate that in the high-frequency limit every bead–spring element, regardless of its drag coefficient, behaves in an identical fashion.

(2) The OFB properties (both magnitude and phase) of 2a are remarkably similar to those of 1a. On the other hand, 2b has a lower predicted steady flow birefringence than 1b; this is responsible for chain 2 having a lower steady-flow birefringence as well as a higher θ_P peak than chain 1 in Figure 12.

(3) The θ_P curves of 1a and 1b behave as noted previously for a mechanically uniform chain in that they merge together at $\omega\tau_{N,1} \approx 1$, which is responsible for the θ_P valley of the mechanically uniform chain 1 not being deep in Figure 12. On the other hand, θ_P for 2b goes below θ_P for 2a at higher frequencies, and they approach the high-frequency limit at different frequencies; this is the most important and unique characteristic of a model chain with nonuniform bead drag coefficients. Remarkably, θ_P for 2a merges with θ_P for 1a and θ_P for 1b at $\omega\tau_{N,1} \approx 1$; thus, at high frequencies the A blocks of chain 2 act as though they were part of a mechanically uniform chain with the same total N and with every ρ_i equal to ρ_A (in effect, as chain 1). On the other hand, θ_P for 2b goes into the high-frequency limit at $\omega\tau_{N,2} \approx 1$, a higher frequency than that for chain 1. These peculiar properties of 2a and 2b account for chain 2 (Figure 12) having such a low θ_P valley. Therefore, for the mechanically nonuniform chain condition, $-[\theta - \theta_o]_P$ for a symmetric triblock copolymer can lie well below that for a mechanically uniform and optically uniform model chain (homopolymer) with the same total N.

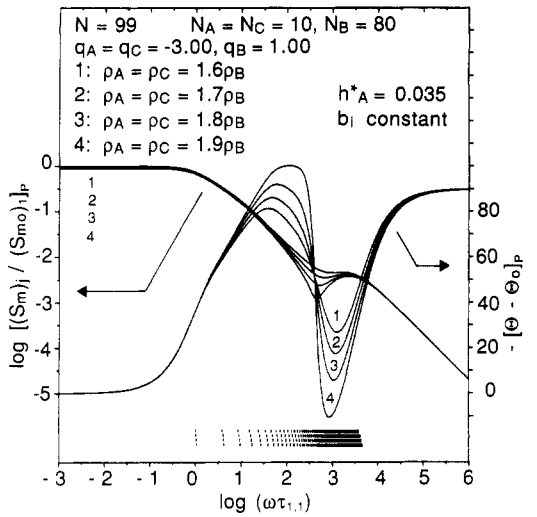

Figure 16. Effect of varying ρ_A/ρ_B on predicted OFB properties for a mechanically nonuniform A–B–A symmetric triblock, with $N = 99$ and $N_A = 10$.

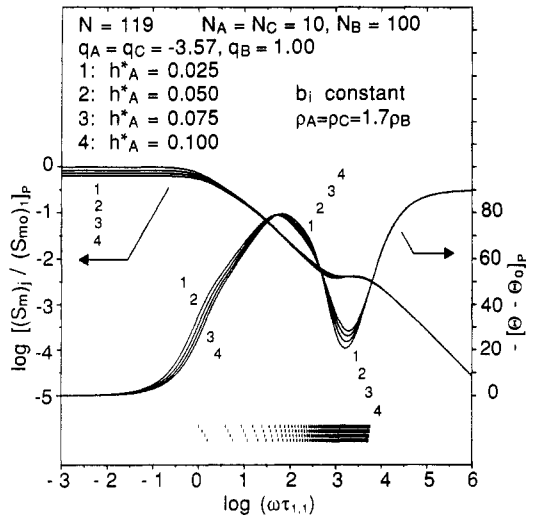

Figure 17. Effect of varying h^* on predicted OFB properties for a mechanically nonuniform A–B–A symmetric triblock, with $N = 119$ and $N_A = 10$.

Figures 16 and 17 present the predicted OFB properties for mechanically nonuniform A–B–A symmetric triblock model chains; in each case only one parameter is varied. Figure 16 illustrates that an incremental increase in ρ_A/ρ_B heightens the phase-angle peak and lowers the phase-angle valley; recall that the major effect is on the π_k/μ_k spectrum, with only a minor effect on the τ_k. Figure 17 illustrates that an incremental increase in h_A^* (also a proportional increase in h_B^*) narrows and slightly raises the phase-angle peak, and lowers the phase-angle valley; here the major effect is the decrease in relaxation time spacings, with only a minor effect on the π_k/μ_k spectrum.

(ii) Diblock. Consider two small diblock model chains (1 and 2) each with $N_A = 8$ and $N_B + N_C = 12$; both chains have been assigned the same optical parameter values of $q_A = -1.25$ and $q_B = q_C = +1.0$. All mean-square spring lengths in the two model chains are the same. The only difference is chain 1 has a uniform bead drag coefficient ($\rho_A = \rho_B = \rho_C$), and chain 2 has nonuniform bead drag coefficients ($\rho_A = 1.5\rho_B = 1.5\rho_C$). To facilitate comparisons between predictions for the two chains, $(\rho_A = \rho_B = \rho_C)_{\text{chain 1}} = (\rho_A)_{\text{chain 2}}$. The OFB predictions for chain 1 and chain 2 for $h^* = 0$, calculated with WMANVB, are shown in Figure 18. The frequency dependences of the normalized OFB

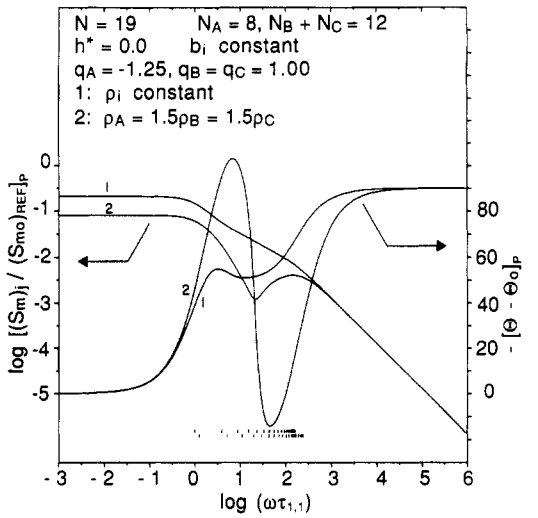

Figure 18. Comparison of predicted OFB properties for a mechanically uniform diblock (curve 1) with those for a mechanically nonuniform but otherwise identical diblock. Magnitude curves normalized as in Figure 6.

contributions from the A component (2a) and B component (2b) for chain 2, each calculated separately, are compared with those (1a and 1b) for chain 1 in Figure 19. Qualitatively, the comparison here between mechanically nonuniform and mechanically uniform diblocks shows essentially the same phenomena as were noted previously for the triblock case; therefore, no additional discussion is necessary here. Furthermore, diblock curves generated by analogy to Figures 16 and 17 for triblocks reveal similar features, and so are not shown.[15]

(iii) Mechanically Nonuniform Block Copolymer Chains: "Exact" Relaxation Times from This Work vs Approximate Relaxation Times from Literature. Some comparisons between exact relaxation times for mechanically nonuniform block copolymers calculated in this work and approximate ones from the literature are presented below.

The *continuous limit* ($N \to \infty$) of the mechanically nonuniform block copolymer chain was investigated by Stockmayer and Kennedy[22] for *free-draining* conditions. This limit is known to be adequate for treating the long-time portion of the relaxation spectrum of a free-draining chain with very large N.[22] In their notation, the numerical bead index j is replaced by the continuous contour variable s, where

$$s = (2j/N) - 1 \tag{37}$$

and therefore the range of s is $-1 \le s \le +1$.

***A*–*B*–*A* Symmetric Triblock.** The B block extends between $s = -\phi$ and $s = +\phi$, with ϕ having a value less than 1. With τ_{1A} and τ_{1B} defined as the terminal relaxation times for an A homopolymer and a B homopolymer, each with the same N as that of the total A–B–A symmetric triblock copolymer under consideration, they derived for the limiting case of a small central block ($\phi \ll 1$) a series expansion that leads to

$$\tau_k/\tau_{kA} = 1 + 2\phi\gamma + \ldots \quad \text{(small } k\text{, odd modes)} \tag{38a}$$

$$\tau_k/\tau_{kA} = 1 + 2\phi\delta + \ldots \quad \text{(small } k\text{, even modes)} \tag{38b}$$

where $\gamma = (b_B^2 - b_A^2)/b_A^2$ and $\delta = (\rho_B - \rho_A)/\rho_A$. Fundamentally equivalent equations were also obtained by Hall and De Wames.[23] The exact eigenvalues λ'_k (thus also ratios of τ_k) have been calculated here for the following

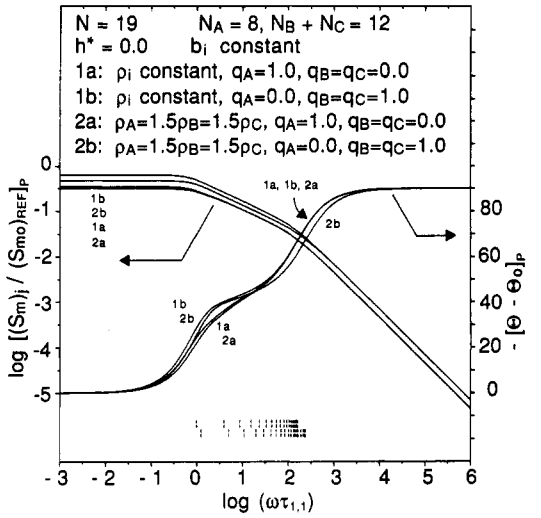

Figure 19. Comparison of predicted OFB contributions from the *A* and *B* blocks (curves 1a and 1b) of a mechanically uniform diblock with those for a mechanically nonuniform but otherwise identical diblock (curves 2a and 2b). Magnitude curves normalized as in Figure 6.

Table I
Comparison of the Exact Eigenvalues, λ_k, with the Predictions of Equations 29a and 39

k	exact λ'_k	exact λ_{kA}, eq 29a	approx λ'_k, eq 39
1	0.000 986 1	0.000 948 6	0.000 986 5
2	0.003 650 4	0.003 793 3	0.003 650 2
3	0.008 869 0	0.008 531 6	0.008 872 3
4	0.014 605 7	0.015 159 0	0.014 587 2
5	0.024 603 6	0.023 669 1	0.024 614 3
6	0.032 873 7	0.034 053 8	0.032 769 2
7	0.048 127 9	0.046 303 4	0.048 152 5
8	0.058 455 2	0.060 406 1	0.058 127 5
9	0.079 349 1	0.076 348 7	0.079 397 6
10	0.091 330 8	0.094 116 0	0.090 565 8
⋮	⋮	⋮	⋮
50	1.955 091 3	1.938 409 9	1.865 290 5
⋮	⋮	⋮	⋮
97	3.988 466 2	3.976 330 9	4.135 119 5
98	3.995 689 6	3.984 841 0	3.834 527 5
99	3.997 324 2	3.991 468 4	4.150 861 5
100	4.199 787 2	3.996 206 7	3.845 464 5
101	51.020 408 2	3.999 051 4	4.158 747 3

unique symmetric triblock copolymer: $N = 101$, $N_A = N_C = 50$, $N_B = 2$, $h_A^* = 0$, $b_A^2/b_B^2 = b_C^2/b_B^2 = 50$, $\rho_A/\rho_B = \rho_C/\rho_B = 0.5$ (*A* block is identical with *C* block), for direct comparison with the above analytic expressions. Significantly, the comparisons for higher mode numbers will demonstrate the interesting and unexpected behavior of local motions of the mechanically nonuniform bead–spring chain. Selected λ'_k values for the above model chain obtained with the WMANVB program are listed in Table I. The only nonuniformity of this particular chain is due to the very small *B* block at the center of the long chain; therefore, eqs 38a and b derived by Stockmayer and Kennedy should be applicable; they predict the following:[22]

$$\lambda_{kA}/\lambda'_k = \tau_k/\tau_{kA} = 1 - 0.0384 \quad \text{for small odd } k \quad \text{(first-order approximation)} \quad (39a)$$

and

$$\lambda_{kA}/\lambda'_k = \tau_k/\tau_{kA} = 1 + 0.0392 \quad \text{for small even } k \quad \text{(first-order approximation)} \quad (39b)$$

Recall that τ_{kA} are the relaxation times for an *A* homopolymer with the same size as the overall triblock under consideration; for this case $N = 101$ and $h^* = 0$, and the inverse of τ_{kA} can be calculated exactly by eq 29a.

The four columns of Table I list the mode index k, the exact λ'_k calculated with the WMANVB, the exact λ_{kA} for the equal N *A* homopolymer, and the approximate λ'_k calculated with the expressions of Stockmayer and Kennedy,[22] for selected values of k.

Some conclusions can be drawn from these results.

(1) The simple first-order predictions derived by Stockmayer and Kennedy[22] (also those by Hall and De Wames)[23] work quite well. From their derivations, we also gain considerable physical insight. The lower odd-numbered modes are affected mainly by the spring constant of the small central *B* block since these modes all have a displacement nodal point at the chain center. Lower even-numbered modes are affected mainly by the drag coefficient of the small central *B* block, since these modes all have a displacement envelope maximum point at the chain center.

(2) For the intermediate modes, as expected, the approximate relations no longer hold. Interestingly, the intermediate λ'_k are closer to λ_{kA} as k increases; for example, λ'_{99} for the triblock is between $\lambda_{100,A}$ and $\lambda_{101,A}$ for the equal N *A* homopolymer. However, an interesting phenomenon appears for the most local motions. The two largest eigenvalues, λ'_{100} and λ'_{101}, for the triblock seem to be "split-off" from the rest and appear to correlate more with the small, more mobile *B* block (two beads) in the copolymer. The peculiarly large λ'_{N-1} and λ'_N (thus peculiarly small τ_{N-1} and τ_N) evidently take on a disproportionally large amount of the character of the *B*-type bead–spring elements (for this case $\rho_A b_A^2 = 25\rho_B b_B^2$).

Other exact eigenvalue calculations with WMAN or WMANVB have been performed for different block structures (different lengths and locations and block mechanical properties).[15] They all consistently show that the relaxation time spectrum is split into as many small groupings of relaxation times as there are different mechanical species in the block copolymer, a phenomenon also observed by Hansen and Shen.[24]

IV. Summary

Bead–spring model calculations have been performed for the polymer contributions to the viscoelastic and oscillatory flow birefringence properties of very dilute block copolymer solutions. The original BSM of Rouse[5] and Zimm[6] has been extended to the case of diblock and triblock copolymers, following the model of Wang.[13,14] The VE properties are determined via exact calculations of the eigenvalues of the modified $\tilde{H}\cdot\tilde{A}$ matrix, for arbitrary values of the parameters N_i, b_i, and ρ_i (and therefore h_i^*), where N_i is the number of beads in block i, b_i is the root-mean-square end-to-end length of a spring in block i, and ρ_i is the friction coefficient of each bead in block i; h_i^* is the hydrodynamic interaction parameter associated with block i. The total number of beads in the chain, N, can assume values up to at least 10^3. Calculation of the OFB properties requires determination of the eigenvectors of the modified $\tilde{H}\cdot\tilde{A}$ matrix, in addition to the eigenvalues, in order to calculate the optical weighting factors, π_k/μ_k, for each of the normal modes. These depend strongly on the relative values of q_i, the optical constant for block i. The q_i are proportional to the stress-optic coefficients for homopolymers of the constituent blocks, while the optical weighting factors may be viewed as effective stress-optic coefficients for the normal modes.

Illustrative calculations for four different situations have been presented. In all cases, it is found that the VE properties are not substantially altered from the homopoly-

mer case, as also reported by Wang.[13,14] The OFB properties, however, can vary strikingly with relatively modest changes in model parameters. This is a direct consequence of the behavior of the optical weighting factors. In the first case, mechanically uniform (constant b and ρ) free-draining ($h^* = 0$) diblocks and triblocks were considered. In this limit, it is possible to derive analytical expressions for the optical weighting factors, which permit some insight to be gained into the frequency dependence of the OFB properties.

In the second set of results, chains with $N = 20$ and for which only one subsection has a nonzero q were examined. By varying the location of the "labeled" section, it is possible to determine the relative contributions of various parts of the chain as a function of frequency. It is found, for example, that, at the highest frequencies, all subchains contribute equally, but that, in the low-frequency limit, subchains in the center of the model molecule contribute relatively more.

In the third case, mechanically uniform diblocks and symmetric triblocks were reexamined, with variable h_i^* and with q_A and q_B of opposite sign. This situation, i.e., block copolymers for which the constituent homopolymers have stress-optic coefficients of different sign, is common; polystyrene–polyisoprene, polystyrene–poly(1,4-butadiene), and polystyrene–poly(methyl methacrylate) all fall into this category. It is found that the OFB properties, particularly the phase angle between the birefringence and the shear rate, can have frequency dependences that are much more featured than their homopolymer equivalents; again, this stems directly from the optical weighting factors, which can now change sign from mode to mode. This behavior offers the possibility that the OFB properties of block copolymer solutions may provide extremely powerful and unique characterization information, in terms of block lengths and locations.

In the final section, mechanically nonuniform diblocks and symmetric triblocks were considered. In general, the conclusions from the previous section are underscored and even enhanced; it is found that small variations between the subchain friction coefficients can lead to even more striking frequency dependences in the birefringence phase angle. In addition, some comparisons were made between the exact eigenvalues calculated here and approximate expressions available in the literature.[22,23] The calculated properties presented in this paper represent a small fraction of the detailed studies carried out; see ref 15 for additional information. In a subsequent publication, the predictions of the block copolymer BSM with mechanically nonuniform chains will be compared with VE and OFB measurements on polystyrene–polyisoprene and polystyrene–poly(1,4-butadiene) solutions.[18]

Acknowledgment. This work was supported by the National Science Foundation Polymers Program through Grants DMR-7925020, DMR-8303207, and DMR-8800641 (J.L.S.) and DMR-8715391 (T.P.L.). We also thank Mr. Donald M. Parsons and Dr. Susanna Amelar for assistance with several of the figures.

References and Notes

(1) See, for example: Bates, F. S.; Fredrickson, G. H. *Annu. Rev. Phys. Chem.* **1990**, *41*, 525, and references therein.
(2) See, for example: Matsushita, Y.; Nakao, Y.; Shimizu, K.; Noda, I.; Nagasawa, K. *Macromolecules* **1988**, *21*, 2790, and references therein.
(3) See, for example: Ferry, J. D. *Viscoelastic Properties of Polymers*; Wiley-Interscience: New York, 1980; and references therein.
(4) See, for example: Martel, C. J. T.; Lodge, T. P.; Dibbs, M. G.; Stokich, T. M., Jr.; Sammler, R. L.; Carriere, C. J.; Schrag, J. L. *Faraday Symp. Chem. Soc.* **1983**, *No. 18*, 173, and references therein.
(5) Rouse, P. E. *J. Chem. Phys.* **1953**, *21*, 1272.
(6) Zimm, B. H. *J. Chem. Phys.* **1956**, *24*, 269.
(7) Lodge, A. S.; Wu, Y. *Rheol. Acta* **1971**, *10*, 539.
(8) Lodge, A. S.; Wu. Y. *Rheology Research Center Report No.* 16, University of Wisconsin, 1972.
(9) Sammler, R. L.; Schrag, J. L. *Macromolecules* **1988**, *21*, 1132.
(10) Sammler, R. L.; Schrag, J. L. *Macromolecules* **1988**, *21*, 3273.
(11) Sammler, R. L.; Schrag, J. L. *Macromolecules* **1989**, *22*, 3435.
(12) Soli, A. L. Ph.D. Thesis, University of Wisconsin, 1978.
(13) Wang, F. W. *Macromolecules* **1975**, *8*, 364.
(14) Wang, F. W. *Macromolecules* **1978**, *11*, 1198.
(15) Man, V. F. Ph.D. Thesis, University of Wisconsin, 1984.
(16) Stokich, T. M., Jr. Ph.D. Thesis, University of Wisconsin, 1988.
(17) Morris, R. L.; Amelar, S.; Lodge, T. P. *J. Chem. Phys.* **1988**, *89*, 6523.
(18) Man, V. F.; Soli, A. L.; Schrag, J. L.; Lodge, T. P., manuscript in preparation.
(19) Kirkwood, J. G.; Riseman, J. *J. Chem. Phys.* **1948**, *16*, 565.
(20) Thurston, G. B.; Peterlin, A. *J. Chem. Phys.* **1967**, *46*, 4881.
(21) Thurston, G. B.; Morrison, J. B. *Polymer* **1969**, *10*, 421.
(22) Stockmayer, W. H.; Kennedy, J. W. *Macromolecules* **1975**, *8*, 351.
(23) Hall, W. F.; De Wames, R. E. *Macromolecules* **1975**, *8*, 349.
(24) Hansen, D. R.; Shen, M. *Macromolecules* **1975**, *8*, 343.